Technical University of Denmark

DTU

Optical fiber link for transmission of 1-nJ femtosecond laser pulses at 1550 nm

Eichhorn, Finn; Olsson, Rasmus Kjelsmark; Buron, Jonas Christian Due; Grüner-Nielsen, Lars; Pedersen, Jens Engholm; Jepsen, Peter Uhd

Link back to DTU Orbit

DTU Library
Technical Information Center of Denmark

Optical fiber link for transmission of 1-nJ femtosecond laser pulses at 1550 nm

Finn Eichhorn[1], Rasmus Kjelsmark Olsson[1], Jonas C. D. Buron[1], Lars Grüner-Nielsen[2], Jens Engholm Pedersen[3], and Peter Uhd Jepsen[1]*

[1]*DTU Fotonik, Technical University of Denmark, DK-2800 Lyngby, Denmark*
[2]*OFS Fitel Denmark Aps, Priorparken 680, DK-2605 Brøndby, Denmark*
[3]*NKT Photonics A/S, Blokken 84, DK-3460 Birkerød, Denmark*
*puje@fotonik.dtu.dk

Abstract: We report on numerical and experimental characterization of the performance of a fiber link optimized for the delivery of sub-100-fs laser pulses at 1550 nm over several meters of fiber. We investigate the power handling capacity of the link, and demonstrate all-fiber delivery of 1-nJ pulses over a distance of 5.3 m. The fiber link consists of dispersion-compensating fiber (DCF) and standard single-mode fiber. The optical pulses at different positions in the fiber link are measured using frequency-resolved optical gating (FROG). The results are compared with numerical simulations of the pulse propagation based on the generalized nonlinear Schrödinger equation. The high input power capacity of the fiber link allows the splitting and distribution of femtosecond pulses to an array of fibers with applications in multi-channel fiber-coupled terahertz time-domain spectroscopy and imaging systems. We demonstrate THz pulse generation and detection using a distributed fiber link with 32 channels and 2.6 nJ input pulse energy.

References and Links

1. W. R. Zipfel, R. M. Williams, and W. W. Webb, "Nonlinear magic: multiphoton microscopy in the biosciences," Nat. Biotechnol. **21**(11), 1369–1377 (2003).
2. M. Tonouchi, "Cutting-edge terahertz technology," Nat. Photonics **1**(2), 97–105 (2007).
3. W. L. Chan, J. Deibel, and D. M. Mittleman, "Imaging with terahertz radiation," Rep. Prog. Phys. **70**(8), 1325–1379 (2007).
4. C. Lin, H. Kogelnik, and L. G. Cohen, "Optical-pulse equalization of low-dispersion transmission in single-mode fibers in the 1.3 - 1.7-microm spectral region," Opt. Lett. **5**(11), 476–478 (1980).
5. L. Grüner-Nielsen, M. Wandel, P. Kristensen, C. Jørgensen, L. V. Jørgensen, B. Edvold, B. Palsdottir, and D. Jakobsen, "Dispersion-Compensating Fibers," J. Lightwave Technol. **23**(11), 3566–3579 (2005).
6. C. C. Chang, A. M. Weiner, A. M. Vengsarkar, and D. W. Peckham, "Broadband fiber dispersion compensation for sub-100-fs pulses with a compression ratio of 300," Opt. Lett. **21**(15), 1141–1143 (1996).
7. D. G. Ouzounov, K. D. Moll, M. A. Foster, W. R. Zipfel, W. W. Webb, and A. L. Gaeta, "Delivery of nanojoule femtosecond pulses through large-core microstructured fibers," Opt. Lett. **27**(17), 1513–1515 (2002).
8. J. M. Dudley, L. P. Barry, P. G. Bollond, J. D. Harvey, and R. Leonhardt, "Characterizing Pulse Propagation in Optical Fibers around 1550 nm Using Frequency-Resolved Optical Gating," Opt. Fiber Technol. **4**(3), 237–265 (1998).
9. J. S. Skibina, R. Iliew, J. Bethge, M. Bock, D. Fischer, V. I. Beloglasov, R. Wedell, and G. Steinmeyer, "A chirped photonic-crystal fibre," Nat. Photonics **2**(11), 679–683 (2008).
10. J. V. Rudd, D. A. Zimdars, and M. W. Warmuth, "Compact fiber-pigtailed terahertz imaging system," Proc. SPIE **3934**, 27–35 (2000).
11. I. Duling, and D. Zimdars, "Compact TD-THz systems offer flexible, turnkey imaging solutions," Laser Focus World **43**, 63 (2007).
12. B. Sartorius, H. Roehle, H. Künzel, J. Böttcher, M. Schlak, D. Stanze, H. Venghaus, and M. Schell, "All-fiber terahertz time-domain spectrometer operating at 1.5 microm telecom wavelengths," Opt. Express **16**(13), 9565–9570 (2008).
13. V. Krozer, T. Löffler, P. U. Jepsen, F. Eichhorn, R. K. Olsson, J. D. Buron, J. Dall, A. Kusk, V. Zhurbenko, and T. Jensen, "THz Imaging Systems with Aperture Synthesis Techniques," submitted to IEEE Trans. Microwave Theory Tech. (2009).

14. K. W. DeLong, R. Trebino, J. Hunter, and W. E. White, "Frequency-resolved optical gating with the use of second-harmonic generation," J. Opt. Soc. Am. B **11**(11), 2206–2215 (1994).
15. G. P. Agrawal, *Nonlinear Fiber Optic,* 4th ed. (Academic Press, 2006).
16. http://www.photonics.umd.edu/software/ssprop/

Introduction

Delivery of nJ, sub-100-fs laser pulses via an all-fiber distribution link has many applications in multi-photon microscopy [1], terahertz spectroscopy [2] and terahertz imaging [3] as well as in other areas where beam delivery of fs-pulses via optical fiber is of an advantage. All-fiber pulse compression schemes are also of interest for fiber amplifier systems where it can replace bulk optics prism or grating compressors.

Dispersion management of sub-100-fs pulses in the linear regime using dispersion-compensating fiber (DCF) at 1300 nm to 1700 nm wavelength has originally been proposed by Lin *et al*. [4] and was treated in a review of DCF fibers by Grüner-Nielsen *et al.* [5]. Chang *et al*. [6] demonstrated nearly dispersion-free transmission of sub-100-fs pulses in the low picojoule energy range over a 42 m concatenated single-mode fiber (SMF) - DCF fiber link. In this and similar dispersion compensation experiments the idea is to match the dispersion of the SMF with the dispersion of a piece of DCF that has the same magnitude but is opposite in sign. For very short pulses or long fiber lengths the third-order dispersion (TOD) has to be efficiently compensated as well. Since the pulse peak power in these experiments was low, nonlinear effects were negligible.

Pulse delivery of nanojoule femtosecond pulses through large-mode-area (LMA) fibers has been demonstrated by Gaeta *et al.* [7]. Here 3 nJ pre-chirped input pulses were compressed to 140 fs, and it was demonstrated that LMA fiber under the same conditions delivered 10 times shorter pulses than standard SMF due to reduced self-phase modulation (SPM).

Propagation in standard and dispersion-shifted fibers around 1550 nm has been studied experimentally using frequency-resolved optical gating (FROG) [8]. The FROG technique allows a detailed characterization of higher-order soliton evolution and pulse propagation near the zero dispersion wavelength of an optical fiber.

Recent work on pulse delivery of sub-100-fs, < 800 nm pulses with microjoule pulse energies in specialty hollow core PCF has been demonstrated by Skibina *et al.* [9]. The chirped HC-PCF fiber showed very low dispersion enabling delivery of pulses with duration as short as 26 fs through 1 m fiber, without further dispersion management.

Terahertz time-domain spectroscopy (THz-TDS) and THz-imaging using photoconductive switches are two areas within the terahertz field with an increasing amount of emerging applications [2,3]. One limiting factor on the application side is the complexity of the free-space optical systems requiring ultrafast lasers pulses (< 100 fs) to pump and probe the THz emitters and detectors, respectively. The field has advanced with respect to robustness and applicability with the advent of more simple fiber-pigtailed measuring setups using movable fiber-coupled emitters and detectors. Zimdars *et al.* [10] avoided first free-space optics in their fiber-pigtailed THz sensor heads by pre-chirping the ultrafast laser pulses in an external grating compressor prior to fiber-launch. An existing commercial version is the Picometrix T-Ray 4000 TD-THz System [11].

Sartorius *et al.* recently demonstrated an all-fiber THz-TDS system using low-temperature-grown InGaAs/InAlAs multi-layer photoconductive switches [12]. In this system, a pulsed fiber laser operating at 1550 nm delivered 100-fs, sub-nJ pulses which were precompensated inside the laser unit for 10 m single-mode fiber.

Another application of a fiber based distribution link is that it enables multi-channel THz systems by using fiber splitters to distribute the pulses throughout the network. The sub-100-fs pulses are then fed into an array of individual photoconductive switches which generate or detect THz radiation [13].

In this paper we explore all-fiber dispersion management for the 1.55-µm wavelength range, with special emphasis on the transition from low-power propagation where standard dispersive effects determine the final pulse duration, to high-power propagation where

nonlinear effects and, in particular, SPM become decisive for the pulse quality at the output of the fiber link. We demonstrate transmission of pulses at 1 nJ energy which are compressed to sub-100 fs duration. We observe that SPM has a significant effect of the compression. In our experiments the input pulse is the positively chirped output from an amplified Er-doped fiber laser. We initially stretch the pulse further in DCF fiber and then compress it to its final duration in several meters of standard single-mode fiber. The fiber link is characterized by measuring the pulses at different positions in the fiber link in a cutback experiment and using second-harmonic frequency resolved optical gating (SHG-FROG) for pulse retrieval [14]. Finally we demonstrate that by increasing the input energy to 2.6 nJ and splitting the fiber link into 32 channels, the link can be an important component for distribution of femtosecond laser pulses to arrays of THz antennas.

The advantages of the approach presented here for the 1.55-µm wavelength range are the straight forward low-loss fusion splicing techniques for telecom fibers, and the availability of low-cost of-the-shelf fibers and standard components such as isolators and power splitters.

Fiber link design

The fiber link is designed to deliver nJ sub-100 fs pulses after a few meters of optical fiber (see Fig. 1). The link consist of 0.56 m EWB DCF (extra-wide-band DCF) [5] which is pigtailed with 20 cm SMF at each end and then spliced onto approximately 5 m of standard SMF. The DCF is a standard component in dispersion-managed cables in low-power telecom applications. The DCF has a high dispersion parameter D and a high nonlinear coefficient γ because of a small mode area. The dispersion of the DCF fiber is normal at 1550 nm, with a relative dispersion slope (RDS) precisely matched to that of standard SMF. The fiber parameters are summarized in Table 1. The splice loss for each of the two splices between SMF and DCF is 0.3 dB. A FC/APC connector is spliced onto the input fiber such that the total length of SMF fiber before the DCF fiber is 37.5 cm. The optimum length of the final SMF fiber in the fiber link will depend on the energy of the pulse. The optimum length for our purposes is determined in fiber cutback measurements and the results are shown below.

Fig. 1. Fiber link design. The output of the fiber laser is butt-coupled to the fiber link using FC/APC connectors. The crosses show where SMF and DCF fiber sections are spliced together.

After the first small piece of SMF fiber, the positively chirped input pulse is further stretched in the DCF fiber section. This increases the total length of the fiber link from approximately 0.7 m without additional DCF to more than 5 m with 0.56 m of DCF. The additional stretching of the pulse after the DCF section also offers a point in the fiber link with relatively low peak power of the pulse. At this point, additional fiber elements with limited peak power capability can be inserted with the lowest risk of optical damage. In the last section of the paper we will demonstrate this by inserting a 1x32 power splitter based on planar glass waveguide technology in the fiber link. After the DCF section the pulse is compressed to its shortest duration in standard single-mode fiber due to a combination of anomalous dispersion and SPM [15].

Characterization of the fiber laser input

The femtosecond light source that is used in the experiments is an FFS.SYS mode-locked 1550 nm fiber laser from TOPTICA Photonics AG. The system was originally designed to deliver 100 fs pulses into free space with an average power of 250 mW. We removed the free-space prism compressor inside the laser and replaced it by an FC/APC connector spliced directly on the output of the amplifier section of the fiber laser. The fiber laser output, i.e. the

input to the fiber link, was characterized by FROG after the FC/APC connector as shown in Fig. 2. The FROG retrieval errors were typically on the order of 1-3% for this and all other FROG traces reported here, with 256^2 points in the FROG spectrogram. The phase of the input pulse is nearly quadratic with a negative curvature, which shows that it has a linear and positive chirp. The input pulse has a full-width-at-half-maximum (FWHM) duration of 0.8 ps and a center wavelength around 1550 nm.

Table 1. Fiber parameters at 1550 nm.

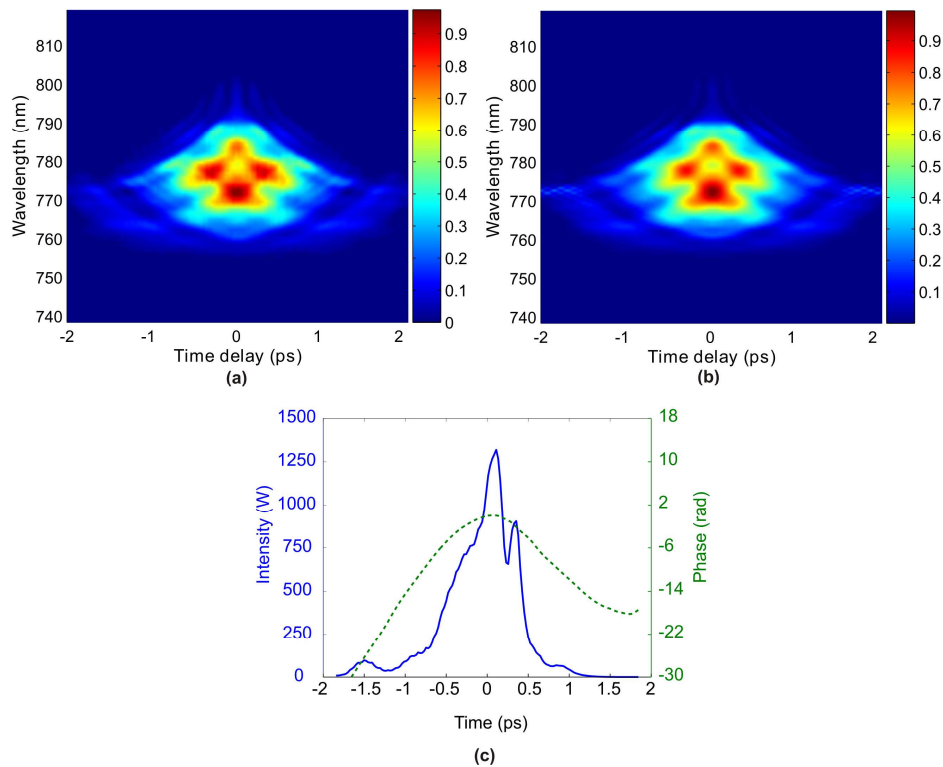|	Dispersion, D (ps/nm/km)	Dispersion slope, S (ps/nm²/km)	Relative dispersion slope, RDS	Effective area, A_{eff} (μm²)	Nonlinear coefficient, γ ($W^{-1}km^{-1}$)
Standard single mode fiber (SMF), ITU G652	16.5	0.058	$3.5 \cdot 10^{-3}$	82	1.29
Dispersion compensating fiber (DCF), EWBDK	−120	−0.44	$3.6 \cdot 10^{-3}$	21	5.02

Fig. 2. FROG characterization of the 1-nJ input pulse. (a) Measured spectrogram and (b) spectrogram of the retrieved pulse. The intensity is normalized to the maximum intensity of each spectrogram. (c) The retrieved pulse intensity (solid, blue curve) and phase (green, dashed curve).

Fiber link simulation results

Pulse propagation through the fiber link is numerically simulated using the generalized nonlinear Schrödinger equation [15], using the experimentally measured input pulse and fiber parameters shown in Table 1. We have used the software library SSPROP [16] for the pulse

propagation simulations. The numerical simulations solves the nonlinear Schrödinger equation,

$$\frac{\partial u}{dz} + \frac{\alpha}{2}u + i\frac{\beta_2}{2}\frac{\partial^2 u}{\partial t^2} - \frac{\beta_3}{6}\frac{\partial^3 u}{\partial t^3} = i\gamma\left(|u|^2 u + i\frac{t_0}{2\pi}\frac{\partial\left(|u|^2 u\right)}{\partial t} - T_R u\frac{\partial\left(|u|^2\right)}{\partial t}\right), \qquad (1)$$

where u is the slowly varying pulse envelope $u(z, t)$ in the reference frame moving along with the pulse at the group velocity, $t = t_0 - z/v_g$ where t_0 is the physical time, and where it is assumed that the electric field propagates in the positive z-direction. The simulations include β_2 and β_3 which are the expansions coefficients of the propagation constant. The nonlinear terms in left hand side of Eq. (1) describe the Kerr effect, self-steepening, and stimulated Raman scattering. T_R in equation Eq. (1) represents the Raman response. The nonlinear parameter γ is defined as

$$\gamma = \frac{2\pi n_2}{A_{eff}\lambda_0} = \frac{n_2\omega_0}{cA_{eff}}, \qquad (2)$$

where n_2 is the nonlinear refractive index coefficient and A_{eff} the effective modal area of the fiber.

Figure 3 shows the results of a numerical propagation of a pulse with low energy (0.1 nJ), and a pulse with higher energy (1.0 nJ). In the low energy case the compression is mainly due to dispersion, and the pulse is compressed to a FWHM duration of 122 fs at the position 5.67 m in the fiber link. The length of the waist region where the pulse is shortest can be defined as the distance between the positions in the fiber link where the pulse is stretched to $\sqrt{2}FWHM(L_{min})$ where $FWHM(L_{min})$ is the FWHM duration at the minimum position. For the 0.1 nJ pulse this waist region is 95 cm long. In the 1 nJ case the pulse is compressed at an earlier position in the fiber link due to a combination of dispersion and self-phase modulation [15]. The pulse is compressed to a FWHM duration of 57 fs at the position 5.26 m. The region of the fiber link where the pulse is short is only 28 cm long and after this the pulse breaks up into several pulses.
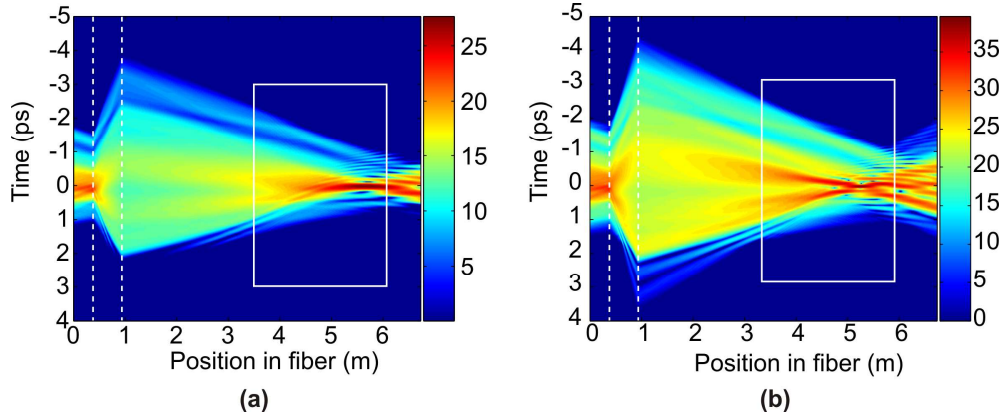

Fig. 3. Numerical simulation of the pulse propagating through the fiber link with 0.1-nJ input pulse (a) and a 1.0-nJ input pulse (b). The pulse intensity is shown as a function of time and position in fiber link. The intensity scale is in dBW. The white dashed lines indicate the different fiber sections and the white boxes indicate the area where the experimental data is obtained.

Fiber link measurements

The output of the DCF section of the fiber link was measured for different input pulse energies. A small length of SMF was used to couple the light into the measurement setup and the measured pulses correspond to the pulses at position 1.66 m in the fiber link. The energy of the input pulse was adjusted by changing the coupling efficiency in the butt coupling between the fiber laser and the fiber link. The results for 0.1-nJ and 1.0-nJ pulses are shown in Fig. 4. Although minor differences in the pulse shape can be seen when the energy is increased, the overall pulse characteristics after the DCF does not change significantly when the pulse energy is increased from 0.1 to 1.0 nJ, indicating that linear dispersion dominates over SPM in this part of the link, even at 1.0-nJ pulse energy.
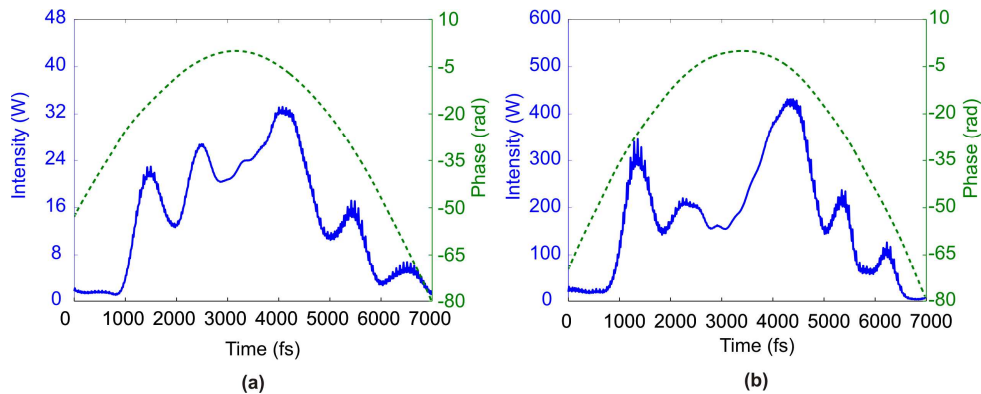

Fig. 4. Measured pulses after the DCF fiber for a 0.1 nJ pulse (a) and a 1.0 nJ pulse (b).

The pulse evolution and compression in the SMF fiber was measured in a detailed fiber cutback experiment. Starting at a length of 6.0 m of the fiber link, each cutback removed a few centimeters of fiber and the output pulses were measured for different pulse energies. The fiber piece was cut out from the middle of the SMF fiber and the fiber ends were spliced together again. In this way it was possible to keep the output coupling into the measurement setup fixed. The results for 0.1-nJ and 1.0-nJ pulses are shown in Fig. 5. Since there is no absolute phase information in the SHG-FROG measurements we had to manually align the individual pulses in time with respect to one another. There is a time ambiguity in the SHG-FROG technique and it is not possible a priori to know if a retrieved pulse is oriented correctly on the time axis or if it should be flipped in time. However, here the sign of the chirp of the input pulse is known from the fact that the pulse is compressed in the anomalous dispersive fiber. The retrieved pulse is oriented on the time axis such that the chirp has the same sign. The pulses that follow in the fiber link are oriented in time in the same way and aligned with respect to the input pulse.

We see a very good qualitative agreement between the evolution of the pulse shape seen in the experiment (Fig. 5) and in the simulation (Fig. 3). In the low-power case the shortest possible pulse is compressed with a pulse shape which approaches a single peak. The slower compression of the wings of the pulse is visible both in the simulation and the experiment, and there is little pulse break-up after the point of shortest pulse duration. In the high power link, the pulse with the shortest duration consists of several peaks, and we observe a significant reduction of the length of the region where the pulse is short, as well as a strong break-up of the pulse after the point of shortest duration.
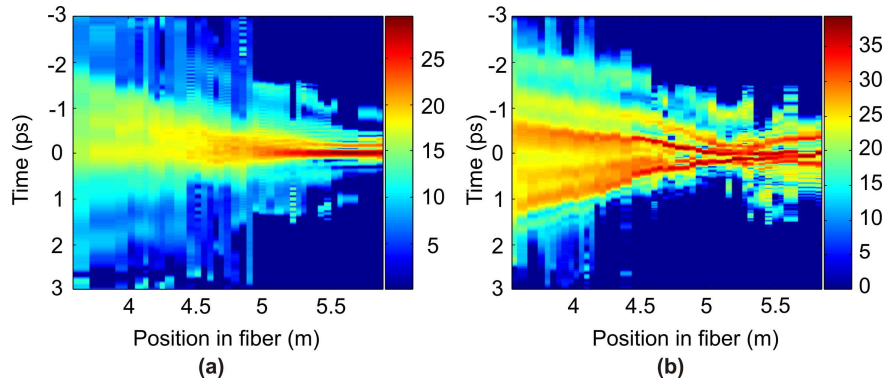
Fig. 5. Experimental measurements of 0.1 nJ (a) and 1.0 nJ (b) pulses showing the final stage of the compression in the SMF fiber. The pulse intensity is shown as a function of time (vertical axis) and position (horizontal axis) in fiber link. The intensity scale is in dBW.

Figure 6 shows the pulses at the optimum position in the fiber link where the pulses are shortest and where most of the pulse energy is in the center peak. The 0.1-nJ pulse is compressed to a FWHM duration of 84 fs and a peak power of 0.9 kW at 5.62 m which is close to the expected position. The 1.0-nJ pulse is compressed to its shortest duration at 5.27 m, with a FWHM duration of less than 60 fs but with significant energy in the side pulses. The peak power is 6.9 kW.
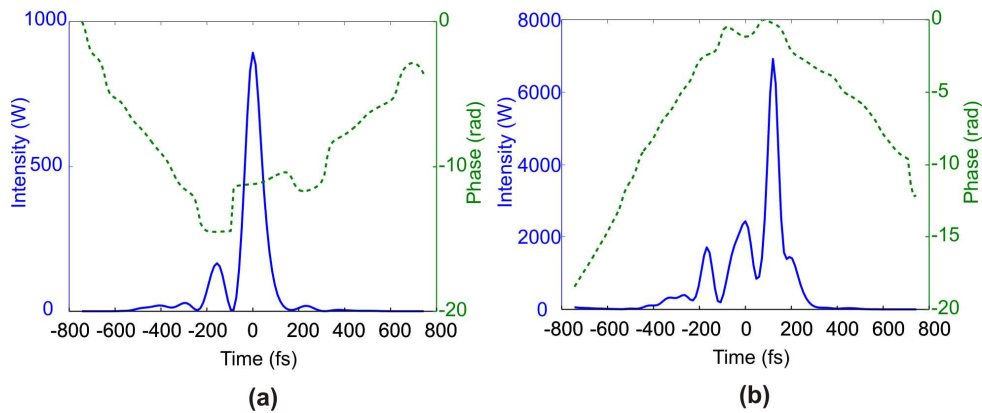

Fig. 6. The optimum 0.1 nJ (a) and 1 nJ (b) pulses. The pulse envelope (solid line) and phase (dashed line) are shown.

For this fiber link the main power-handling limitation is the effect that the pulse breaks up into several pulses when the pulse energy is increased. For pulse energies higher than 1.0 nJ we have seen, both numerically and experimentally, significant pulse breakup and it was not possible to compress and obtain sufficient energy in the main pulse.

Fiber link for multi-element terahertz imaging

The close similarity between the pulses after the DCF section of the fiber, shown in Fig. 4, indicates that the input pulse energy might be increased even further. A further increase of the input pulse energy will enable an extension to the simple 1x1 link demonstrated in the previous section. By introducing a 1x32 fiber splitter (Ignis Photonyx PLC 1x32) into the fiber link and increasing the pulse energy to 2.6 nJ we are able to provide 32 channels of 100 fs pulses, each with a pulse energy of 0.06 nJ (corresponding to 5 mW average power), sufficient to drive 32 photoconductive THz emitters or detectors. Figure 7 shows the fiber link design.
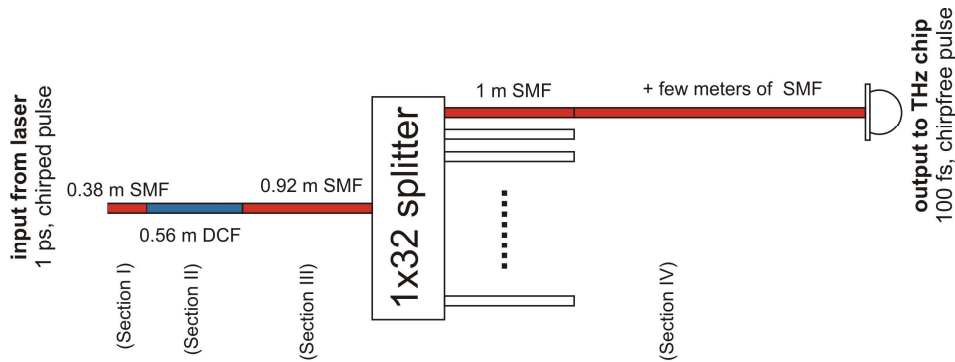
Fig. 7. Design approach of the multiple-element fiber link between the femtosecond laser and the THz antennas.

Figure 8(a) depicts the simulated pulse intensity along the fiber link, again using the measured output pulse from the laser as input to the simulation. The pulse is compressed in Section I which is SMF and stretched in the DCF part of Section II. The abrupt change in intensity after Section III is due to the 1x32 fiber splitter. Again using the measured input pulse, the simulations show that the pulse can be compressed to a FWHM duration of 100 fs after a total length of 5.65 m fiber. The compressed pulse is shown in Fig. 8(b).
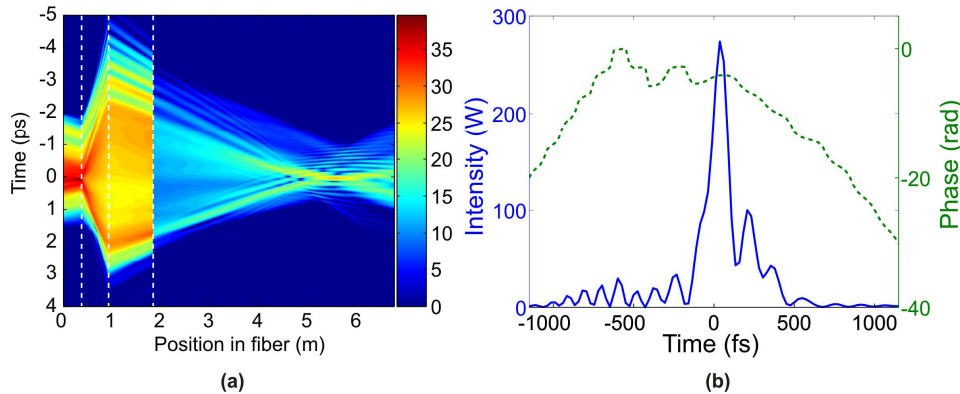

Fig. 8. (a) 2D plot on a logarithmic scale (dBW) of the simulated pulse intensity as a function of fiber length using the measured output pulse from the laser as input pulse. The dashed line indicates the borderline between the different fiber sections. (b) Plot of the intensity and the phase of the simulated compressed pulse at 5.65 m. The FWHM pulse length is 100 fs.

As in the previous section, the simulation results are validated in a fiber cutback experiment. We have recorded autocorrelation traces for various fiber lengths, across the area where the numerical simulations predicted a minimum pulse length. Figure 9(b) shows a zoomed-in view of the measured autocorrelation functions as function of fiber link. A minimum is seen at about 5.8 m of total fiber link length. At this point the pulse is shortest and the fiber should be terminated and attached to the THz antennas. The development of the autocorrelations along the minimum pulse length shows by comparing the two plots in Fig. 9 for numerical data (a) and measured (b), respectively, very similar features before and after the full compression point. These features are present despite the deviation in the fiber link lengths. The minimum measured autocorrelation FWHM is 99 fs (~80 fs pulse length) at 5.8 m link length. The simulated autocorrelations of the real input pulse from the laser reaches a minimum FWHM of 135 fs at the position of 5.65 m.
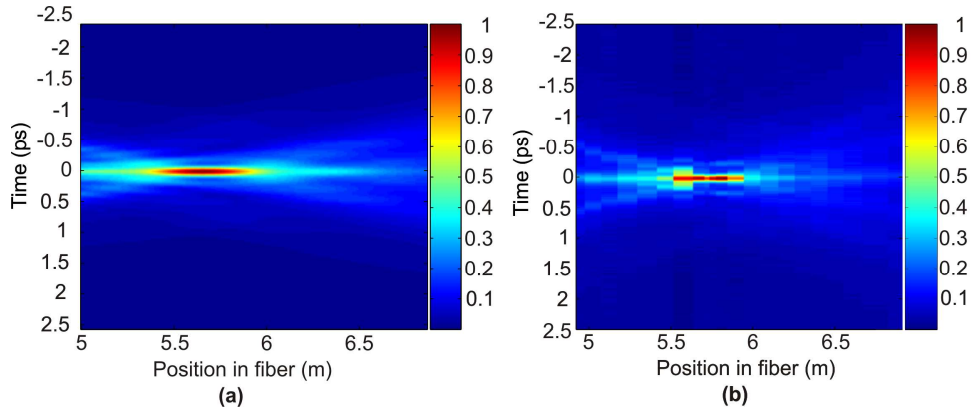
Fig. 9. (a) Simulated autocorrelation functions of pulses in the fiber link at positions near the point where the pulse gets re-compressed to sub-100 fs pulse length. (b) The measured autocorrelation functions in the cutback experiment. The plots are on a linear intensity scale.

Figure 10 shows a measured (a) and retrieved (b) FROG trace of the shortest pulse recorded at a position of 5.8 m. The retrieved FROG trace is in good agreement with the measured trace, and exhibits a FROG retrieval error of 1%.
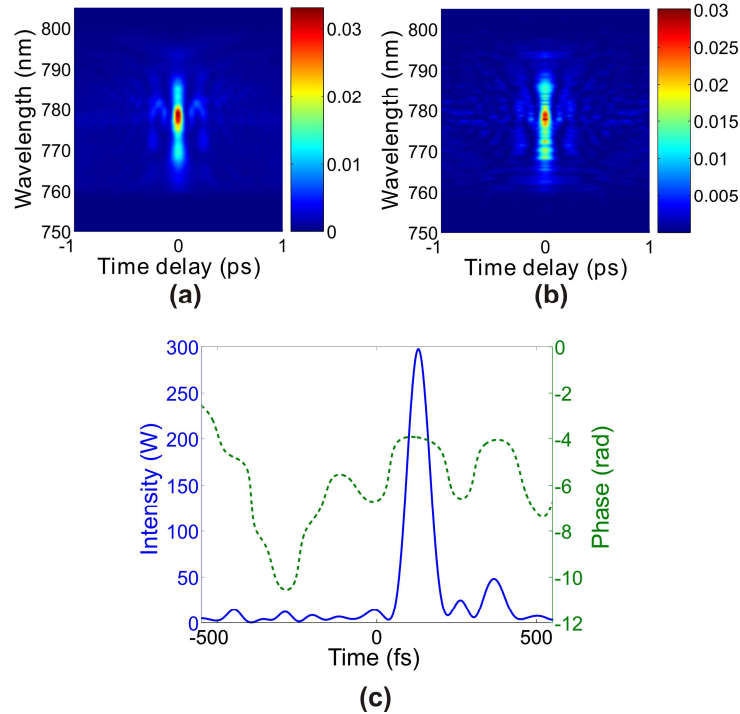

Fig. 10. FROG characterization of the minimum pulse width. Top row: (a) Measured spectrogram and (b) spectrogram of the retrieved pulse. The intensity is normalized to the maximum intensity of each spectrogram. (c) Plot of the intensity and the phase of the measured retrieved pulse at 5.8 m link length.

The retrieved pulse intensity and phase are shown in Fig. 10(c). The extracted pulse intensity exhibit ripples in the trailing edge indicating a complex pulse structure which is expected due to the complex input pulse shape (cf. Fig. 2), and we find excellent agreement with simulation (Fig. 8).

The difference in fiber link length between the measured data and the numerical simulations is 15 cm out of 5.6 m of fiber. We regard this 2.7% deviation as acceptable and it may be explained by uncertainties in the determination of the fiber link input pulse, which showed a FROG-error of approximately 2%, and uncertainties connected to the fiber dispersion along the fiber link. The simulated fiber link length is highly sensitive to variations in the dispersion parameters and the active area of the used fiber.

THz pulse generation with the fiber link

We used the output of the fiber link for generation and detection of THz pulses in a standard THz time-domain spectrometer, by excitation of photoconductive dipole antennas fabricated on InGaAs/AlGaAs superlattice structures [12], commercially available from Menlo Systems. Figure 11 shows the generated THz pulse in the time domain and in the frequency domain. The THz pulse has a near-single-cycle appearance in the time domain, and a corresponding smooth frequency spectrum spanning the range 0.1-2 THz.
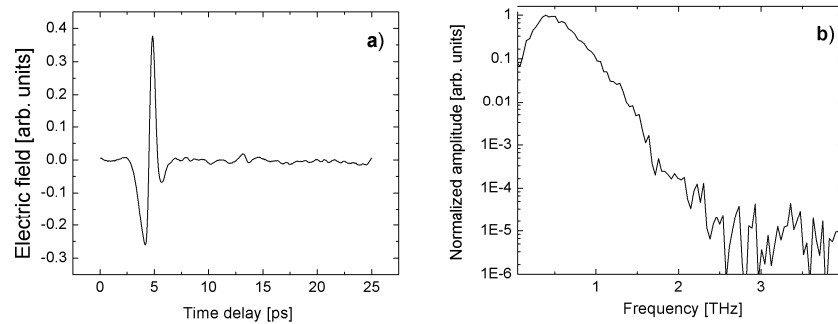

Fig. 11. (a) THz transient in the time domain and (b) its frequency spectrum generated and detected in photoconductive switches excited by 0.06-nJ pulses from the fiber link.

The spectral amplitude of the generated THz signal has a peak dynamic range of approximately 200, corresponding to 50-dB dynamic range in power. The measurement was done by lock-in detection and chopping of the bias voltage on the emitter at a frequency of 3.2 kHz.

Conclusion

We have demonstrated a fiber link consisting of dispersion-compensating fiber and standard single-mode fiber which can transmit sub-100-fs pulses with energy up to 1 nJ. Our simulations and experimental characterization of the evolution of the pulse shape during the propagation in the fiber link are in good agreement, and we observe the onset of nonlinear effects due to self-phase modulation, resulting in pulse break-up and significant reduction of the optimum length of the fiber link.

Using high input pulse energies of several nJ we demonstrated that the fiber link is useful for distribution of femtosecond pulses to as much as 32 parallel outputs, with application for instance in advanced multi-element THz systems.

Acknowledgements